Magnetism in AV_3Sb_5 (A = Cs, Rb, and K): Origin and Consequences for the Strongly Correlated Phases

Md. Nur Hasan,[1] Ritadip Bharati,[2] Johan Hellsvik,[3] Anna Delin,[4,5] Samir Kumar Pal,[1] Anders Bergman,[6] Shivalika Sharma,[7] Igor Di Marco,[6,7,8] Manuel Pereiro,[6] Patrik Thunström,[6] Peter M. Oppeneer,[6] Olle Eriksson,[6,*] and Debjani Karmakar[6,9,†]

[1]*Department of Chemical and Biological Sciences, S. N. Bose National Centre for Basic Sciences, Block JD, Sector-III, SaltLake, Kolkata 700 106, India*
[2]*School of Physical Sciences, National Institute of Science Education and Research HBNI, Jatni—752050, Odisha, India*
[3]*PDC Center for High Performance Computing, KTH Royal Institute of Technology, SE-100 44 Stockholm, Sweden*
[4]*Department of Applied Physics, KTH Royal Institute of Technology, SE-106 91 Stockholm, Sweden*
[5]*Swedish e-Science Research Center (SeRC), KTH Royal Institute of Technology, SE-10044 Stockholm, Sweden*
[6]*Department of Physics and Astronomy, Uppsala University, Box 516, SE-751 20 Uppsala, Sweden*
[7]*Asia Pacific Center for Theoretical Physics, Pohang 37673, Republic of Korea*
[8]*Department of Physics, Pohang University of Science and Technology, Pohang 37673, Republic of Korea*
[9]*Technical Physics Division, Bhabha Atomic Research Centre, Mumbai 400085, India*

(Received 17 May 2023; accepted 28 September 2023; published 9 November 2023)

The V-based kagome systems AV_3Sb_5 (A = Cs, Rb, and K) are unique by virtue of the intricate interplay of nontrivial electronic structure, topology, and intriguing fermiology, rendering them to be a playground of many mutually dependent exotic phases like charge-order and superconductivity. Despite numerous recent studies, the interconnection of magnetism and other complex collective phenomena in these systems has yet not arrived at any conclusion. Using first-principles tools, we demonstrate that their electronic structures, complex fermiologies and phonon dispersions are strongly influenced by the interplay of dynamic electron correlations, nontrivial spin-polarization and spin-orbit coupling. An investigation of the first-principles-derived intersite magnetic exchanges with the complementary analysis of q dependence of the electronic response functions and the electron-phonon coupling indicate that the system conforms as a frustrated spin cluster, where the occurrence of the charge-order phase is intimately related to the mechanism of electron-phonon coupling, rather than the Fermi-surface nesting.

DOI: 10.1103/PhysRevLett.131.196702

The V-based kagome stibnite series AV_3Sb_5 (A = Cs, Rb, and K), or V135 in short, has acquired a center-stage in the community of topological materials, paralleling twisted bilayer graphene and high T_c cuprates [1,2]. Here, the interplay of strong correlation and nontrivial topology leads to a plethora of exotic phases, harbouring translational, rotational and time-reversal symmetry breaking. The electronic dispersion of AV_3Sb_5 displays strongly correlated features near the Fermi energy (E_F), e.g., the flatbands of V-d character, van Hove singularities (vHS) at the Brillouin-zone-boundary [3] and nontrivial topological Dirac crossing of the bands hosting vHS [4]. Their fermiologies are related to the presence of charge bond order (CBO) instability, where the triplet orbital nature ($l = 1$) of the particle-hole wave function bears a contrast to the conventional charge-density wave (CDW) of particle-hole singlets ($l = 0$) [3]. Prior works associated this CBO with the sublattice interference and 3Q-nesting behavior [5,6], promoting a nematic chiral charge order and spontaneously breaking both the time reversal and the C_6 rotational symmetry [3,7].

Topological Dirac electrons under strong electron correlation and spontaneous symmetry breaking prepare the playground of a co-existing panoply of unconventional and interrelated charge-ordered (CO) and superconducting (SC) phases for V135 compounds [8–10]. The CO-phase emerges at 80–100 K (T_{CO}) and the SC-phase pertains a critical temperature (T_c) of ∼1–3 K [9,10]. Spectroscopic imaging detects a complex landscape of superlattice reconstructions related to the CO [1], where the bulk charge-order comprises of a $2 \times 2 \times 4$ superlattice with inverse star of David (ISD) pattern in the kagome plane and three consecutive layers of star-of-David (SD) pattern [11,12].

In the scientific community, there is a lack of consensus regarding whether the CO phase is competing with the SC phase, trying to gap-out the same band crossings by similar

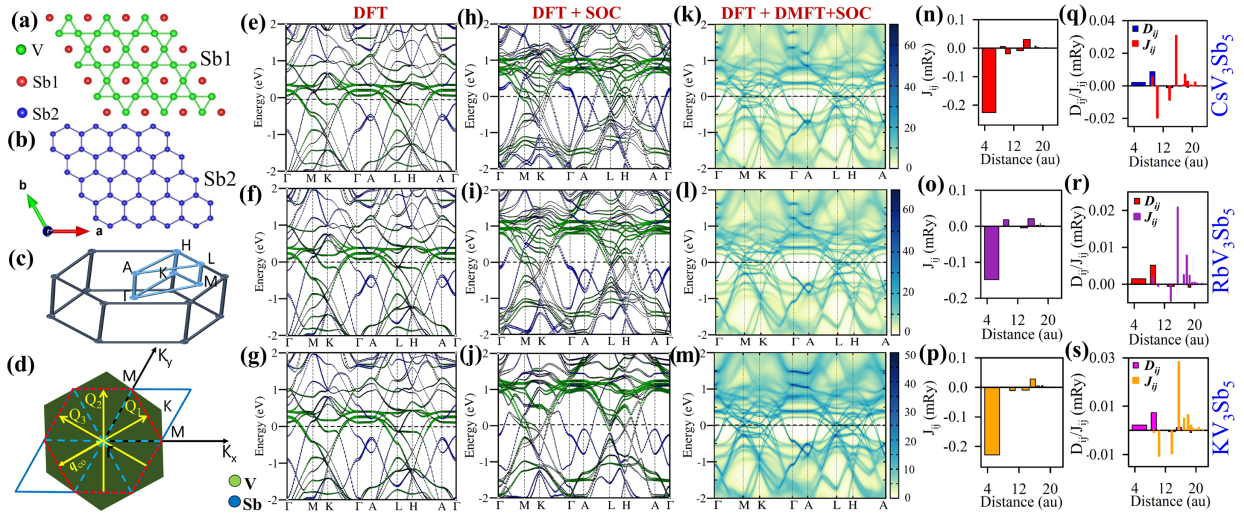

FIG. 1. (a) V_3Sb1-kagome sublattice and (b) the Sb2 honeycomb sublattice, (c) the hexagonal Brillouin zone (BZ), (d) The 2D BZ (green-filled hexagon), the k-space unit cell (blue parallelogram), one ideal FS sheet (red dotted line) and the 3Q-nesting vectors (yellow) with magnitude shown as q_{CO}, (e)–(g) The atom-projected band structures for AV_3Sb_5 by spin-polarized DFT, (h)–(j) corresponding atom-projected band structures with the spin-polarized DFT + SOC and (k)–(m) corresponding electronic spectral function with the spin-polarized DFT + DMFT + SOC method at 78 K, color scale representing the band-broadening related to quasiparticle lifetimes. (n)–(p) J_{ij} and (q)–(s) D_{ij} for AV_3Sb_5. In (q)–(s), the J_{ij} values are in the same plot, except for the first NN.

electronic instabilities or if the former is a precursor of the latter [9,13–16]. There is also a long-standing debate about the pairing symmetry associated with the SC phase. The available explorations constitute a wide variety of reports on the types of superconducting gaps [17,18] and the corresponding pairing symmetries [19–26].

The presence of local moments and the impact of magnetism on the correlated aspects are not investigated in detail for AV_3Sb_5. The V-3d states could have been empty in the V_3Sb_5 network with valence levels V^{5+} and Sb^{3-}, unless the alkali-metal (A) donates a single electron to the kagome net. This single delocalized electron and its hybridization with Sb-5p_z set the stage for the intriguing correlated electron physics. Experimentally, the temperature dependence of the magnetization is consistent with the Curie-Weiss behavior at high temperature with an effective magnetic moment of $\sim 0.22\ \mu_B$ per V [10]. In principle, if the V ions are capable of sustaining a local moment, a spin-bond order with a finite angular momentum should compete energetically with CBO.

Whereas measurements like muon-spin depolarization in polycrystalline samples divulge negligible local moments [27], for single crystals, there is a striking enhancement of the internal field below T_{CO}, implying the presence of a time-reversal symmetry breaking [28]. The most puzzling aspect of AV_3Sb_5 is the presence of giant anomalous Hall effect (AHE) with anomalous Hall ratio being an order of magnitude higher than that of Fe [29,30]. Conventionally, magnetic topological materials evince an intrinsic AHE related to the Berry phase [31,32]. For these systems, experimental prediction demanded the origin of the AHE to be extrinsic [29,30], where the electrons undergo an enhanced skew scattering due to the magnetic fluctuations in the triangular spin clusters, as proposed in the "spin cluster" model by Ishizuka and Nagaosa [33]. The prior studies focused on the non-spin-polarized Fermi-surface (FS)-nesting between the electron pockets to the mode softening at the same value of the displacements (q), indicating a structural instability, which disappears under a $2 \times 2 \times 2$ reconstruction for KV_3Sb_5 [34] with a simultaneous exodus of imaginary modes. To the best of our knowledge, the magnetic attributes of these systems have received much less attention. Employing first-principles electronic structure, phonon, and time-dependent density functional theory (TDDFT) calculations, we have explored the impacts of electronic correlations and magnetism on their complex nontrivial physical properties.

In the V135 series (symmetry-group $P6/mmm$), the hexagonal A layer intercalates the quasi-2D network of the V_3Sb1-kagome and the Sb2-honeycomb sub-lattices, as in Figs. 1(a) and 1(b). The corresponding 2D-Brillouin zone (BZ) with an ideal schematic sheet of the FS and nesting vectors (to be discussed below) are presented in Figs. 1(c) and 1(d). With inclusion of spin polarization, a survey of energetics for the long-range order reveals that while the out-of-plane magnetic coupling is ferromagnetic (FM), as in Table S1 of the Supplemental Material [35], the different in-plane spin-configurations, as described in Table S2 of the Supplemental Material [35], are energetically comparable, indicating a frustrated nature for the in-plane magnetism. Figures 1(e)–1(m) presents a comparison of the spin-polarized atom-projected band dispersions of CsV_3Sb_5 (CVS), RbV_3Sb_5 (RVS), and KV_3Sb_5 (KVS) in the FM configuration, using three different

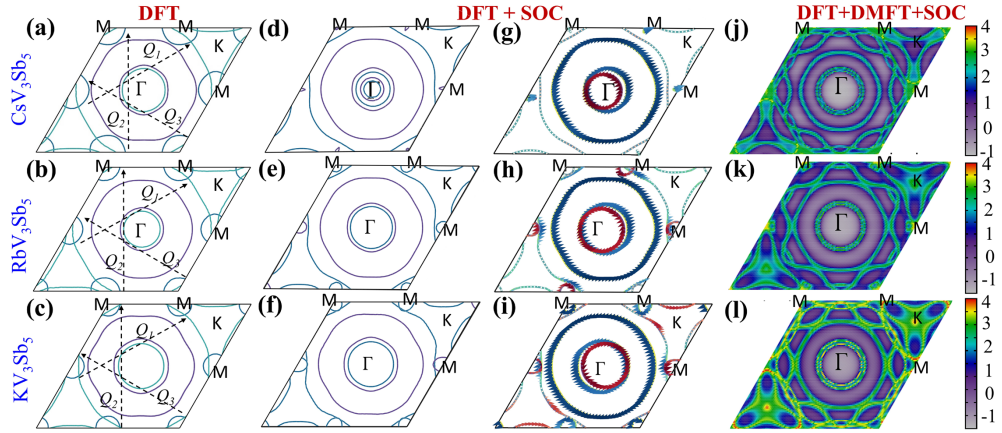

FIG. 2. (a)–(c) 2D FS of AV_3Sb_5 from spin-polarized DFT. The dotted arrow shows the 3Q nesting behaviour. (d)–(f) 2D FS and (g)–(i) spin-textures from DFT + SOC. The red and blue colors signify the spin-up and spin-down projections. (j)–(1) the 2D FS from DFT + DMFT + SOC. The color bar represents the Fermi velocity.

methodologies [35], viz., (I) density-functional theory (DFT), (II) DFT including the spin-orbit coupling (SOC), and (III) DFT+dynamical mean-field theory (DMFT)+SOC, respectively. Figure 2 presents the 2D projections of their respective Fermi-surfaces in the [001] plane. The intricate outcomes of this comparative study can be categorized as: (I) In the collinearly spin-polarized DFT bands [Figs. 1(e)–1(g)], the featured signatures constitutes a quasi-2D Γ-centered electron pocket from the Sb-5p_z states, multiple vHS at the M-point from the V-d_{xy} and V-$d_{xz/yz}$ orbitals and the near-E_F Dirac crossing (DC) at the K-point [45]. The corresponding [001]-projected 2D-FS in Figs. 2(a)–2(c), are composed of one Γ-centred 2D sheet, one quasi-2D sheet, constituting both the Γ-centered 2D-pocket and 3D-flares near the corners of the BZ, and the 3D M-centered electron pockets related to the vH filling of the V-d levels. These pockets are precisely responsible for the 3Q nesting as in Figs. 2(a)–2(c). In Fig. S1 of the Supplemental Material, the band-projected FS sheets are presented [35]. (II) In DFT + SOC, the inclusion of SOC couples the magnetism to the real space, leading to moments along all three spin axes as in Table S3 [35] of the Supplemental Material. The resultant magnetic moment, being higher than the experimental value, indicates the necessity of a better treatment of the dynamical electronic correlations. The exchange splitting and the associated energy shift push the flat bands away from E_F, bring the DCs closer to it, modify the vH filling while also creating new vHS with higher orders [35] and change the area of crossing of the Sb-5p_z bands (blue) near A point [Figs. 1(h)–1(j)]. In Figs. 2(d)–2(f), the most notable changes occur at the vH-points. The M-centered electron pockets almost disappear for CVS, while a reduction of area is observed for RVS and KVS. The effect of spin polarization is also asserted from the spin-texture-projected FS in Figs. 2(g)–2(i). (III) For dynamically correlated metals, the state-of-the-art treatment of the local electronic correlations can be obtained by the merger of DFT with the DMFT [46], based on a self-consistent multiband Anderson-impurity model. This model is solved by the fully relativistic spin-polarized T-matrix fluctuation-exchange (SPTF) solver [47,48], which is efficient for moderately correlated metals with onsite Coulomb correlation $U \leq W/2$ (W being the bandwidth) [49–51]. The electron temperature is kept as 78 K ($<T_{CO}$). Figures 1(k)–1(m) represents the k-resolved correlated electronic spectral functions, where the broadening reflects the quasiparticle lifetimes derived from the imaginary part of the self-energy [51]. Compared to the DFT + SOC, there is an overall flattening of the bands leading to a significant reduction of the bandwidth with a consequential modification of the low-energy band structure around E_F, where the flat V-d levels [green bands in Figs. 1(h)–1(j) below 1 eV] cross the Sb-5p_z electron pockets and the area of the inverted band crossings of Sb-5p_z bands is remarkably reduced. The mass enhancements of the carriers corresponding to the V-d levels are in the moderately correlated range, as calculated from the quasiparticle weight extracted from the imaginary part of the self-energy to be ∼1.7 (Table I). In the v_F-weighted and smeared FS, as in the Figs. 2(j)–2(l), DMFT-induced band renormalizations instigated many additional

TABLE I. (a) Superconducting T_c in K calculated using the EPC in the spin-polarized state from the Allen-Dynes equation, spin moment, and orbital moment of vanadium (V), and the average effective mass (m^*/m_{DFT}) from DFT + DMFT + SOC.

System	Superconducting T_c (K)	Spin moment (μ_B)	Orbital moment (μ_B)	Average effective mass (m^*/m_{DFT})
CsV_3Sb_5	2.44	0.28	0.032	1.71
RbV_3Sb_5	1.14	0.27	0.038	1.68
KV_3Sb_5	0.95	0.28	0.039	1.72

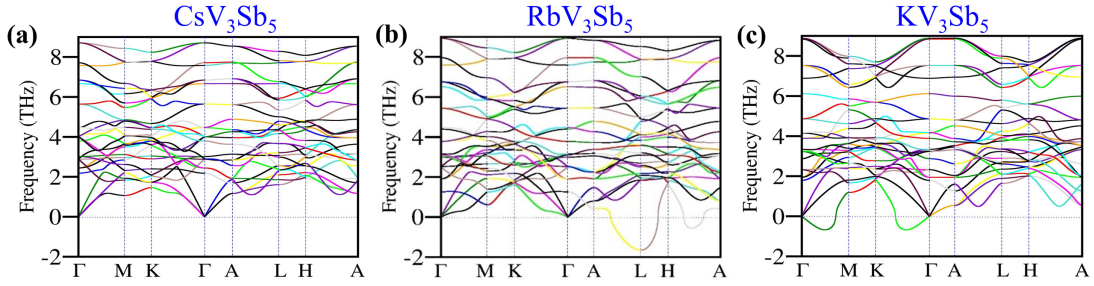

FIG. 3. Phonon dispersion for spin-polarized calculations of (a) CsV_3Sb_5, (b) RbV_3Sb_5, and (c) KV_3Sb_5.

features, viz., occurrence of additional FS sheets, the negligible areas of the M-centered pockets, highest velocity of the carriers for KVS and the transformation of the K-centered triangular electron pocket into a combination of three pockets situated at around $2\pi/3$ apart. The V-d-projected partial spectral functions and the corresponding orbital-projected FS, as presented in Fig. S2 of the Supplemental Material, confirm the contribution of V-d levels towards the dynamical electronic correlation [35].

The significant modifications of the electronic excitations with spin polarization and strong correlation suggest the possibilities of their substantial interplay with the elastic properties and thus may have a crucial impact on exotic phases like CO and SC. From the DFT + DMFT + SOC calculations, the local spin and orbital moments of V possess a small but non-negligible value of $\sim 0.28\ \mu_B$ and $0.032\ \mu_B$, respectively (Table I), which is closer to the experimental values of $0.22\ \mu_B$ [9,10].

Understanding of the role of the local moments of V in the itinerant background of the Dirac-like carriers is fundamental to obtain a complete picture of the low-energy magnetic excitations and their impact on both the elastic and inelastic properties of the correlated electron system. Using the Liechtenstein-Katsnelson-Antropov-Gubanov (LKAG) method [52,53], as implemented in fully relativistic DFT + DMFT + SOC calculations [54,55], the low-lying magnetic excitations are mapped into an effective spin Hamiltonian [54,55] to extract the intersite exchange parameters like the isotropic Heisenberg exchange (J_{ij}) and Dzyaloshinkii-Moriya (D_{ij}) interactions. The calculated magnetocrystalline anisotropies suggest that the alignment of the spin and orbital-moments follows an easy-axis pattern, being along the local magnetic z axis, which is also supported by the spin-component-projected spectral functions, as presented in Fig. S3 of the Supplemental Material. Figures 1(n)–1(p) depict the J_{ij} and D_{ij} parameters as a function of the nearest neighbor (NN) distances in the global coordinate system and imply three important facts, in accordance with the experimental scenario. First, the J_{ij} values are an order of magnitude higher for the first NN as compared with the next ones, suggesting the formation of a spin cluster, as indicated in the AHE experiments [29,30]. Second, the first NN J_{ij}'s are negative, implying that the V spins would prefer to align anti parallel to their NN, which is prevented by the frustration associated with the kagome-lattice-geometry. Third, after the first NN, the J_{ij} and D_{ij} values become comparable in magnitude, as in Figs. 1(q)–1(s), suggesting the plausible presence of a spin-spiral-like magnetic ground state. In a further continuation of the present work, the presence of such complex spin-textures constituting a superposition of spin-spirals are demonstrated [56]. The importance of dynamical correlations in evaluating the exchange properties is reassured from a comparison of the DFT + U and DFT + DMFT results, as seen in Fig. S4 of the Supplemental Material [35]. The electronic moments associated to the itinerant Dirac-like and localized flat bands modify the spin part of the crystal potential, with consequential impacts on the electron-phonon coupling parameter [57,58] and the FS nesting.

The nonmagnetic versus the magnetic phonon dispersions of AV_3Sb_5 at a temperature of ~ 95 K are plotted in Fig. S5 of the Supplemental Material [35] and Fig. 3, respectively. The nonmagnetic phonon dispersions reveal the presence of significant imaginary phonon modes at the M and L points for both RVS and KVS. CVS, on the other hand, does not display any imaginary mode. The lattice displacements at M and L points of RVS and KVS are displayed in *movie 1* of the Supplemental Material [35], indicating the substantial role of the interlayer breathing modes. With spin polarization, CVS continues to be devoid of imaginary modes, as in Fig. 3(a). The absence of the imaginary modes for both magnetic and nonmagnetic CVS poses a question towards the interdependence of CO and FS nesting (FSN). For magnetic RVS and KVS, the reduced frequency of the imaginary modes and the diminished areas of the 3D FS pockets [Figs. 2(e)–2(f)] iterate the same question. The lattice displacements corresponding to the highest imaginary modes for the spin-polarized RVS and KVS are presented in *movie 2*, where traces of the interlayer breathing modes remain evident. In CVS, the relaxed magnetic structure has the smallest c axis in the V135 series, where the intercalated Cs ions forms the heaviest and largest-radii alkali-metal layer, restricting the interlayer breathing modes. Pertinent discussions regarding the microscopic analysis are included in the Supplemental Material [35]. Prior studies of the non-magnetic structures

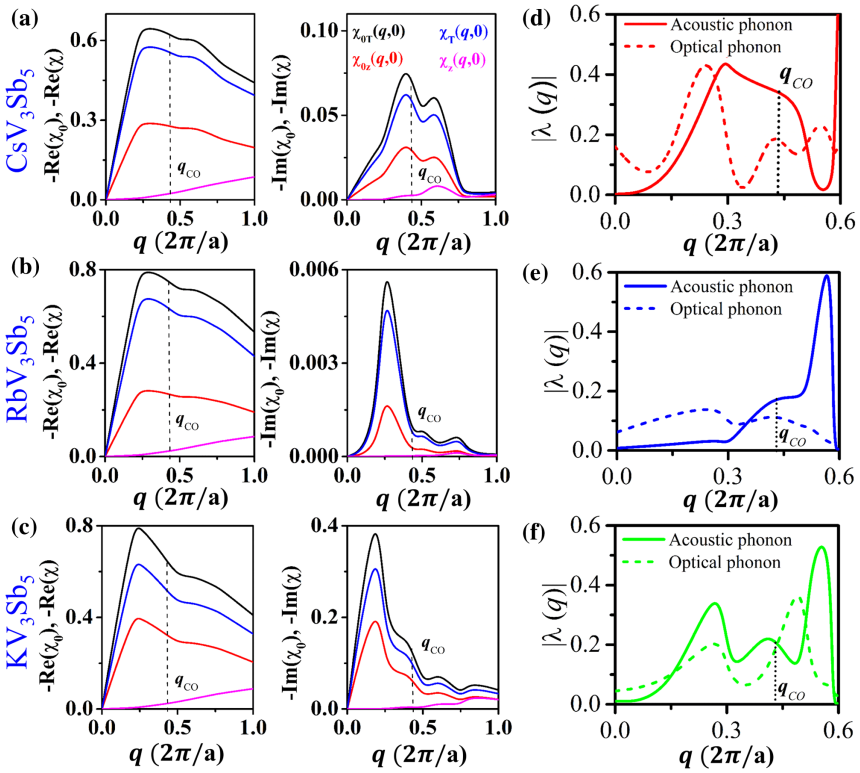

FIG. 4. (a)–(c) The real and imaginary part of the interacting (χ) and noninteracting (χ_0) response functions for the in-plane (χ_T and χ_{0T}) and out-of-plane (χ_z and χ_{0z}) magnetization as $\omega \to 0$, the corresponding colors are displayed as legends; (d)–(f) the EPC matrix elements $|\lambda(q)|$ for the acoustic and optical (multiplied by four) modes as a function of q.

related the softened modes at the nesting-q values to the structural instability and CO [34]. Thus, analysis of the CO, FSN and their interrelation with the electron-phonon coupling (EPC) is imperative to acquire a better understanding.

The influence of the magnetic ordering is apparent from the comparison of mode and spin-averaged Eliashberg spectral functions $[\alpha^2F(\omega)]$ in Fig. S7 in the Supplemental Material [35] for magnetic and nonmagnetic cases. This in turn will impact the electron-phonon (e-ph) matrix elements, as per the Hopfield relation $(\lambda/N_\sigma) = D^2/M\omega^2$ with λ, N_σ, D, and $M\omega^2$ being the e-ph coupling constant, the electronic DOS at E_F, the deformation potential and the force constant respectively. By using the density-functional perturbation theory (DFPT), we have calculated the λ parameters for both configurations and compared the λ, N_σ, (λ/N_σ) and the superconducting T_c values from the Allen and Dynes formulation [59] in Table S4 of the Supplemental Material [35]. The T_c values are closer to the experimental values than those of the spin-degenerate ones, as seen in Table I.

The presence of both FSN and EPC spurs the question of the impact of the respective elastic and inelastic electron-ion scattering on CO. For a 3D system, CO is fundamentally rooted in the electron-ion interaction and thus has an implicit dependence on the electronic response function (χ). Whereas the real part of the response function (Reχ) is connected with the instability causing CO, the imaginary part (Imχ) is coupled to FSN [60]. For systems like $CeTe_3$, where CO is linked to FSN, both Reχ and Imχ display a peak at the magnitude of the nesting vector (q_{CO}) [60]. However, for systems like $NbSe_2$, CO is entirely connected to EPC and the Reχ and Imχ are devoid of any peak at q_{CO} [60–62]. To investigate the underlying cause of CO in AV_3Sb_5, using TDDFT [35], we have plotted the q dependence of the interacting (χ) and noninteracting (χ_0) response functions as $\omega \to 0$ along $\Gamma - M$ for both in-plane and out-of-plane magnetizations in Figs. 4(a)–4(c). Here, the nesting magnitude (q_{CO}) is calculated from the approximate schematic in Fig. 1(d). The presence of a shallow nondivergent peak for Reχ indicates the 3D nature of AV_3Sb_5 and also predicts the presence of a CO. However, the interdependence of this CO and FSN appears extremely fragile as both Re$\chi(\chi_0)$ and Im$\chi(\chi_0)$ refrains to display a peak at q_{CO}) for all three systems. Therefore, the role of EPC in CO needs to be examined.

For systems where the instability connected to the CO phase is linked with the low-frequency acoustic phonon modes, the associated mode softening almost invariably exhibits an explicit presence of imaginary modes. However, for instabilities linked to the higher-frequency acoustic or optical modes having nonzero frequencies at the zone center, it is energetically expensive to obtain a softening after crossing the zero-frequency line. This behavior is also evident for Bi-2212 cuprates with EPC connected to the A^{1g}

TABLE II. Summary of the interplay of exotic phases and various possible coupling factors.

Exotic phases	SP + OP + SOC	DEEC	EPC
CO	(a) SP and OP of V-d + SOC + interplay with itinerant electrons produced flatbands, vHS and Dirac-topology	(a) Proper treatment of DEEC at 78 K ($< T_{CO}$) produced significant band renormalization	(a) Calculated q-dependent EPC has intimate link with CO
	(b) Reconstructed nesting, vanishing M-point pockets	(b) Reproduced frustrated magnetic environment	(b) Indicated the vibrational modes leading to instabilities
	(c) Prepared base for incorporation of DEEC	(c) Extracted J_{ij} and D_{ij} explains experimental scenario	
	(d) Reduced imaginary modes compared to spin-degenerate theory		
SC	(a) $\alpha^2F(\omega)$ displayed impacts of local moments	(a) Higher values of effective masses indicated strong correlation	(a) EPC has relevance for the SC phase and theory reproduces reasonable T_c
	(b) Calculated EPC reproduced experimental T_c, by Allen-Dyne formalism.	(b) Extracted J_{ij} and D_{ij} values are consistent with the measured spontaneous symmetry breaking	(b) Inelastic electron-ion scattering have more impact

optical modes [60–62], as discussed in the Supplemental Material [35].

For AV_3Sb_5, in spite of the experimental evidences of CO, the absence of imaginary modes in CVS instigated the search for the responsible electron-ion phenomena. Therefore, we calculated the q-dependent EPC matrix elements for the acoustic and optical modes corresponding to the largest λ parameters [Figs. 4(d)–4(f)] along $\Gamma - M$. For acoustic modes of CVS, albeit the peak is away from q_{CO}, the EPC around q_{CO} consists of a broad shoulder region. The optical mode, however, is associated with an explicit peak. This nature of EPC implies a larger contribution of the optical modes towards the structural instability. The shoulder at q_{CO} can be attributed to the high-frequency acoustic modes with a nonzero ω, as $q \to 0$. On the contrary, for RVS and KVS, the EPC due to the acoustic modes are more responsible for CO, hosting a corresponding peak near q_{CO}. Here, softening of the low-frequency acoustic modes leads to the imaginary phonon modes. For RVS, the optical modes may also have a smaller contribution, as indicated by the shallow peak for optical modes at q_{CO}. The incommensurate FSN in the kagome systems seems to have lesser impact on the CO. The instability of the underlying electronic subsystem is intricately connected to the vibrational instability of the triangular ionic subsystem.

In summary, using first-principles investigations, we have investigated the microscopic origin of the local magnetic moment in the V-based kagome series and its consequences on the electronic and vibrational properties. The three factors, viz. the spin and orbital polarization with SOC (SP + OP + SOC), dynamical electron-electron correlations (DEEC), and EPC are demonstrated to have overreaching consequences on the exotic phases, as summarized in Table II. Rather than the FSN, the phenomenon of CO in this series is observed to have an intricate dependence on the EPC of the system. In conclusion, the incorporation of magnetism and its interplay with the orbital and vibrational degrees of freedom and their impacts on the correlated aspects are capable of explaining several experimental features and simultaneously widen the panorama of exotic physical properties of kagome superconductors.

Financial support from Vetenskapsrådet (Grants No. VR 2016-05980 and No. VR 2019-05304), and the Knut and Alice Wallenberg foundation (Grants No. 2018.0060, No. 2021.0246, No. 2022.0108, and No. 2022.0079) is acknowledged. The computations were enabled by resources provided by the National Academic Infrastructure for Supercomputing in Sweden (NAISS) and the Swedish National Infrastructure for Computing (SNIC) at NSC and PDC, partially funded by the Swedish Research Council through Grant agreements No. 2022-06725 and No. 2018-05973. O. E. also acknowledges support from ST and UPP, the ERC (FASTCORR project) and eSSENCE. M. N. H. acknowledges CSIR (India) for fellowship. I. D. M. acknowledges support from the JRG Program at APCTP through the Science and Technology Promotion Fund and Lottery Fund of the Korean Government, as well as from the Korean Local Governments-Gyeongsangbuk-do Province and Pohang City. I. D. M. and S. S. also acknowledge financial support from the National Research Foundation of Korea (NRF), funded by the Ministry of Science and ICT (MSIT), through the Mid-Career Grant No. 2020R1A2C101217411. D. K. acknowledges discussion with Debmalya Chakraborty.

*Corresponding author: olle.eriksson@physics.uu.se
†Corresponding author: debjani.karmakar@physics.uu.se

[1] H. Zhao, H. Li, B. R. Ortiz, S. M. L. Teicher, T. Park, M. Ye, Z. Wang, L. Balents, S. D. Wilson, and I. Zeljkovic, Nature (London) **599**, 216 (2021).
[2] J.-X. Yin, B. Lian, and M. Z. Hasan, Nature (London) **612**, 647 (2022).
[3] M. M. Denner, R. Thomale, and T. Neupert, Phys. Rev. Lett. **127**, 217601 (2021).
[4] R. Tazai, Y. Yamakawa, S. Onari, and H. Kontani, Sci. Adv. **8**, eabl4108 (2022).
[5] M. L. Kiesel and R. Thomale, Phys. Rev. B **86**, 121105 (2012).
[6] T. Neupert, M. M. Denner, J.-X. Yin, R. Thomale, and M. Z. Hasan, Nat. Phys. **18**, 137 (2022).
[7] N. Shumiya *et al.*, Phys. Rev. B **104**, 035131 (2021).
[8] I. I. Mazin, H. O. Jeschke, F. Lechermann, H. Lee, M. Fink, R. Thomale, and R. Valentí, Nat. Commun. **5**, 4261 (2014).
[9] B. R. Ortiz, S. M. L. Teicher, Y. Hu, J. L. Zuo, P. M. Sarte, E. C. Schueller, A. M. M. Abeykoon, M. J. Krogstad, S. Rosenkranz, R. Osborn, R. Seshadri, L. Balents, J. He, and S. D. Wilson, Phys. Rev. Lett. **125**, 247002 (2020).
[10] B. R. Ortiz, L. C. Gomes, J. R. Morey, M. Winiarski, M. Bordelon, J. S. Mangum, I. W. H. Oswald, J. A. Rodriguez-Rivera, J. R. Neilson, S. D. Wilson, E. Ertekin, T. M. McQueen, and E. S. Toberer, Phys. Rev. Mater. **3**, 094407 (2019).
[11] Y.-X. Jiang *et al.*, Nat. Mater. **20**, 1353 (2021).
[12] S. Wu, B. R. Ortiz, H. Tan, S. D. Wilson, B. Yan, T. Birol, and G. Blumberg, Phys. Rev. B **105**, 155106 (2022).
[13] Q. Yin, Z. Tu, C. Gong, Y. Fu, S. Yan, and H. Lei, Chin. Phys. Lett. **38**, 037403 (2021).
[14] B. R. Ortiz, P. M. Sarte, E. M. Kenney, M. J. Graf, S. M. L. Teicher, R. Seshadri, and S. D. Wilson, Phys. Rev. Mater. **5**, 034801 (2021).
[15] E. Fradkin, S. A. Kivelson, and J. M. Tranquada, Rev. Mod. Phys. **87**, 457 (2015).
[16] B. Song, X. Kong, W. Xia, Q. Yin, C. Tu, C. Zhao, D. Dai, K. Meng, Z. Tao, and Z. Tu, Nat. Commun. **14**, 2492 (2023).
[17] C. Mu, Q. Yin, Z. Tu, C. Gong, H. Lei, Z. Li, and J. Luo, Chin. Phys. Lett. **38**, 077402 (2021).
[18] X. Wu, T. Schwemmer, T. Müller, A. Consiglio, G. Sangiovanni, D. Di Sante, Y. Iqbal, W. Hanke, A. P. Schnyder, M. M. Denner, M. H. Fischer, T. Neupert, and R. Thomale, Phys. Rev. Lett. **127**, 177001 (2021).
[19] Y. Xiang, Q. Li, Y. Li, W. Xie, H. Yang, Z. Wang, Y. Yao, and H.-H. Wen, Nat. Commun. **12**, 6727 (2021).
[20] S. Ni, S. Ma, Y. Zhang, J. Yuan, H. Yang, Z. Lu, N. Wang, J. Sun, Z. Zhao, and D. Li, Chin. Phys. Lett. **38**, 057403 (2021).
[21] Z. Liang, X. Hou, F. Zhang, W. Ma, P. Wu, Z. Zhang, F. Yu, J. J. Ying, K. Jiang, L. Shan, Z. Wang, and X. H. Chen, Phys. Rev. X **11**, 031026 (2021).
[22] H. Chen *et al.*, Nature (London) **599**, 222 (2021).
[23] Z. X. Wang, Q. Wu, Q. W. Yin, C. S. Gong, Z. J. Tu, T. Lin, Q. M. Liu, L. Y. Shi, S. J. Zhang, D. Wu, H. C. Lei, T. Dong, and N. L. Wang, Phys. Rev. B **104**, 165110 (2021).
[24] H.-S. Xu, Y.-J. Yan, R. Yin, W. Xia, S. Fang, Z. Chen, Y. Li, W. Yang, Y. Guo, and D.-L. Feng, Phys. Rev. Lett. **127**, 187004 (2021).
[25] C. Zhao, L. Wang, W. Xia, Q. Yin, J. Ni, Y. Huang, C. Tu, Z. Tao, Z. Tu, and C. Gong, arXiv:2102.08356.
[26] Y. Gu, Y. Zhang, X. Feng, K. Jiang, and J. Hu, Phys. Rev. B **105**, L100502 (2022).
[27] E. M. Kenney, B. R. Ortiz, C. Wang, S. D. Wilson, and M. J. Graf, J. Phys. Condens. Matter **33**, 235801 (2021).
[28] C. Mielke *et al.*, Nature (London) **602**, 245 (2022).
[29] S.-Y. Yang, Y. Wang, B. R. Ortiz, D. Liu, J. Gayles, E. Derunova, R. Gonzalez-Hernandez, L. Šmejkal, Y. Chen, S. S. P. Parkin, S. D. Wilson, E. S. Toberer, T. McQueen, and M. N. Ali, Sci. Adv. **6**, eabb6003 (2020).
[30] F. H. Yu, T. Wu, Z. Y. Wang, B. Lei, W. Z. Zhuo, J. J. Ying, and X. H. Chen, Phys. Rev. B **104**, L041103 (2021).
[31] Q. Wang, Y. Xu, R. Lou, Z. Liu, M. Li, Y. Huang, D. Shen, H. Weng, S. Wang, and H. Lei, Nat. Commun. **9**, 3681 (2018).
[32] S. N. Guin, K. Manna, J. Noky, S. J. Watzman, C. Fu, N. Kumar, W. Schnelle, C. Shekhar, Y. Sun, J. Gooth, and C. Felser, NPG Asia Mater. **11**, 16 (2019).
[33] H. Ishizuka and N. Nagaosa, Phys. Rev. B **103**, 235148 (2021).
[34] H. Tan, Y. Liu, Z. Wang, and B. Yan, Phys. Rev. Lett. **127**, 046401 (2021).
[35] See Supplemental Material at http://link.aps.org/supplemental/10.1103/PhysRevLett.131.196702 for detailed DFT, DFT + SOC, DFT + DMFT + SOC, inter-site exchange interactions, phonon dispersion, superconducting critical temperature calculations, nonmagnetic phonon dispersion, Eliashberg spectral functions, some supplemental tables, and Refs. [36–44].
[36] J. P. Perdew, K. Burke, and M. Ernzerhof, Phys. Rev. Lett. **77**, 3865 (1996).
[37] G. Kresse and J. Furthmüller, Comput. Mater. Sci. **6**, 15 (1996).
[38] S. Grimme, J. Antony, S. Ehrlich, and H. Krieg, J. Chem. Phys. **132**, 154104 (2010).
[39] A. Grechnev, I. Di Marco, M. I. Katsnelson, A. I. Lichtenstein, J. Wills, and O. Eriksson, Phys. Rev. B **76**, 035107 (2007).
[40] P. Thunström, I. Di Marco, and O. Eriksson, Phys. Rev. Lett. **109**, 186401 (2012).
[41] J. M. Wills, M. Alouani, P. Andersson, A. Delin, O. Eriksson, and O. Grechnyev, *Full-Potential Electronic Structure Method: Energy and Force Calculations with Density Functional and Dynamical Mean Field Theory* (Springer Science & Business Media, New York, 2010), Vol. 167.
[42] A. Togo and I. Tanaka, Scr. Mater. **108**, 1 (2015).
[43] P. Giannozzi *et al.*, J. Phys. Condens. Matter **21**, 395502 (2009).
[44] M. Dadsetani and A. R. Omidi, RSC Adv. **5**, 90559 (2015).
[45] Y. Hu, X. Wu, B. R. Ortiz, S. Ju, X. Han, J. Ma, N. C. Plumb, M. Radovic, R. Thomale, S. D. Wilson, A. P. Schnyder, and M. Shi, Nat. Commun. **13**, 2220 (2022).
[46] A. Georges, G. Kotliar, W. Krauth, and M. J. Rozenberg, Rev. Mod. Phys. **68**, 13 (1996).

[47] L. V. Pourovskii, M. I. Katsnelson, and A. I. Lichtenstein, Phys. Rev. B **72**, 115106 (2005).
[48] M. I. Katsnelson and A. I. Lichtenstein, Eur. Phys. J. B **30**, 9 (2002).
[49] I. Di Marco, J. Minár, S. Chadov, M. I. Katsnelson, H. Ebert, and A. I. Lichtenstein, Phys. Rev. B **79**, 115111 (2009).
[50] M. I. Katsnelson, V. Y. Irkhin, L. Chioncel, A. I. Lichtenstein, and R. A. de Groot, Rev. Mod. Phys. **80**, 315 (2008).
[51] J. Sánchez-Barriga, J. Braun, J. Minár, I. Di Marco, A. Varykhalov, O. Rader, V. Boni, V. Bellini, F. Manghi, H. Ebert, M. I. Katsnelson, A. I. Lichtenstein, O. Eriksson, W. Eberhardt, H. A. Dürr, and J. Fink, Phys. Rev. B **85**, 205109 (2012).
[52] A. I. Liechtenstein, M. I. Katsnelson, V. P. Antropov, and V. A. Gubanov, Magn. Magn. Mater. **67**, 65 (1987).
[53] C. Etz, L. Bergqvist, A. Bergman, A. Taroni, and O. Eriksson, J. Phys. Condens. Matter **27**, 243202 (2015).
[54] Y. O. Kvashnin, O. Grånäs, I. Di Marco, M. I. Katsnelson, A. I. Lichtenstein, and O. Eriksson, Phys. Rev. B **91**, 125133 (2015).
[55] A. Szilva, Y. Kvashnin, E. A. Stepanov, L. Nordström, O. Eriksson, A. I. Lichtenstein, and M. I. Katsnelson, arXiv:2206.02415.
[56] D. Karmakar *et al.*, Phys. Rev. B **108**, 174413 (2023).
[57] L. Boeri, M. Calandra, I. I. Mazin, O. V. Dolgov, and F. Mauri, Phys. Rev. B **82**, 020506 (2010).
[58] F. Yndurain and J. M. Soler, Phys. Rev. B **79**, 134506 (2009).
[59] P. B. Allen and R. C. Dynes, Phys. Rev. B **12**, 905 (1975).
[60] M. D. Johannes and I. I. Mazin, Phys. Rev. B **77**, 165135 (2008).
[61] X. Zhu, Y. Cao, J. Zhang, E. W. Plummer, and J. Guo, Proc. Natl. Acad. Sci. U.S.A. **112**, 2367 (2015).
[62] M. D. Johannes, I. I. Mazin, and C. A. Howells, Phys. Rev. B **73**, 205102 (2006).